Molecular Rydberg States and Ionization Energy Studied by Two-Photon Resonant Ionization Spectroscopy

Yit-Tsong Chen[a,b] (陳逸聰)
[a]*Department of Chemistry, National Taiwan University, Taipei 106, Taiwan, R.O.C.*
[b]*Institute of Atomic and Molecular Sciences, Academia Sinica, P. O. Box 23-166, Taipei 106, Taiwan, R.O.C.*

In this article, I will review the excited valence/Rydberg states and ionization energies of vinyl chloride, propyne, and allyl radical that we have examined recently in our laboratory by 2+1 resonance enhanced multiphoton ionization (REMPI) spectroscopy. In these studies, we have emphasized spectroscopic investigations from the first excited electronic states to the first ionization energies of the molecules and radicals of interest. In spectroscopic analysis, successful electronic identifications have been facilitated with theoretical (*ab initio* and density functional) calculations. In particular, we have applied calculated Franck-Condon factors to assist vibrational assignment for experimental vibronic spectra. The spectroscopic studies of these polyatomic excited valence/Rydberg states help us to illuminate the photodissociation pathways and to manifest the complicated chemical-reaction mechanisms due to the multi-dimensionality in polyatomic molecular potential energy surfaces.

1. INTRODUCTION

Research in the area of molecular excited electronic states covers a broad field of endeavor, touching as it does many aspects in spectroscopy, dynamics/kinetics, photodissociation, and chemical reaction. Potential energy surface (PES) plays a central role in all of these research fields. Taking the study of photodissociation as an example, the topological features of molecular excited electronic PES are closely associated with the mechanisms and outcomes of molecular photodissociation.[1-6] While photodissociation experiments usually measure the internal state, velocity, and angular distribution of photofragments resulting from the characteristics of dissociative PES, spectroscopic investigation of molecular excited states is the most stringent examination to map out the corresponding PES.

In the past four decades, photodissociations of polyatomic molecules excited at convenient wavelengths of 266 nm (4.7 eV; Nd:YAG laser), 248 nm (5.0 eV; KrF laser), 193 nm (6.4 eV; ArF laser), 157 nm (7.9 eV; F_2 laser), and other wavelengths with tunable light sources have been intensively investigated.[1-4] However, polyatomic molecules with their excited electronic PES that have been well characterized spectroscopically are relatively few in number. Many polyatomic molecular PES have so far heavily relied on theoretical calculations without sufficient spectroscopic examination. In molecular photodissociation studies, internal conversion was often presumed for the relaxation of an electronically excited molecule to its ground PES prior to dissociation. This kind of argument was usually concluded from measuring the velocity and angular distribution of photofragments, but the correlated excited states involved in the photodissociation pathways were rarely verified.

From the high-resolution spectroscopic point of view, spectral analysis for rovibronic transitions to the high-lying electronic states of polyatomic molecules is nontrivial, because the high density of electronic states (and/or their companion vibration-rotational levels) and the possible complex-couplings among them could make spectral analysis very difficult. Nevertheless, by judiciously seeking useful experimental elements, spectral complexity can be substantially reduced. In the following discussions, I will simply divide spectroscopic analysis for a rovibronic transition into rotational, vibrational and electronic categories. Discussion of the mutual interactions, e.g., rotation-vibration (Coriolis),[7] vibration-electron (Renner-Teller and Jahn-Teller effects),[7,8] etc., deserves another full chapter and is beyond the scope of this article.

Let us first consider the rotational part in a rovibronic transition. Based on rigorous selection rules originating from the conservation law of angular momentum in physics, rotational quanta involved in a spectral transition can be identified essentially. The correlation between selection rules and physics laws in quantum mechanics, illuminated by C. N. Yang in his Nobel lecture more than four decades ago,[9] is conveyed in Fig. 1. In physics, a symmetry principle (or, equiva-

Dedicated to the celebration of the seventieth anniversary of Chemical Society the located in Taipei.

lently, an invariance principle) generates a conservation law. Quantum mechanically, this renders quantum numbers and corresponding selection rules. In Table 1, we summarize the correlation between conservation law and their corresponding symmetry commonly encountered in molecular spectroscopy. Taking the rotation of a symmetric-top molecule as a representative example, molecular quantum numbers and their corresponding selection rules that we usually visit in high-resolution spectroscopy are listed in Table 2. For instance, the selection rules for angular momentum and parity are such extremely rigorous ones that $\Delta J = 0, \pm 1$ and $+ \leftrightarrow -$ always hold for a dipole-transition in molecule-radiation interaction.

Second, how about molecular electronic and vibrational quantum numbers involved in a spectral transition? Let us consider the electronic part now. Thanks to the advanced development in the computational methods for molecular orbitals,[10-14] molecular excited electronic states with reasonably high excitation energy can nowadays be calculated (under Born-Oppenheimer approximation) to a sufficiently accurate level that can effectively compare with experimental results. Facilitated with the calculated (adiabatic and vertical) electronic excitation energies, geometries and transition dipoles, molecular excited electronic states involved in observed spectra can be identified extensively. To date, even though the convergence for calculating the very high-lying electronic states of polyatomic molecules is still technically difficult and demanding, the electrons somewhat behave in a unique and much simpler manner when they are distant from their molecular core. More specifically, molecular electrons with excitation energy of ≥ 5 eV lie beyond valence orbitals and occupy the so-called Rydberg states. An electron with such a large amount of excitation energy is quite far away from its molecular core which can legitimately be regarded as a positive "point-charge" and a simple hydrogen-like model is suitable for describing the high-lying Rydberg electrons.

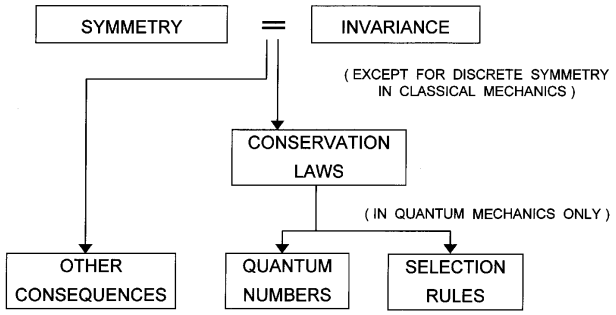

Fig. 1. Relationship between conservation laws and symmetry laws (taken from Ref. 9).

Table 1. Correlation between Symmetry and Conservation Laws

Symmetry	Conservation laws
Isotropy	Angular momentum
Left-right	Parity
Permutation	Nuclear spin modification

Quantum defect theory[15-17] has been developed to portray molecular Rydberg states with an amendment (i.e., an adjustable quantum defect) to the Rydberg formula of a hydrogen atom. Long lifetime and slow motion are salient characteristics for the electrons in Rydberg states.[18-27] When the excitation energy approaches the limit of the first ionization energy (IE), the electron is ready to couple into the ionization channel and leaves the molecular core behind as a cation.

Finally, let us go to molecular vibrations. There is no selection rule tied to any kind of physics conservation laws that are directly associated with molecular vibrations and can intrinsically regulate vibrational motions in a spectral transition. For a pure vibrational transition, it is spectroscopically allowed as long as the vibrational transition-dipole matrix-element is non-diminishing. To the companion vibrational bands in an allowed electronic transition, it is the vibrational overlap integral between the initial and final states (Franck-Condon factors, FCFs) that determines the spectral intensity of each vibrational band. Therefore, identifying vibrational quanta can sometimes become very difficult and challenging, especially for the congested highly-excited vibrational states. By the same token, because of this vibrational integral, vibrational levels of the initial and final electronic states that have similar nuclear geometry will show up preferentially in electronic spectroscopy. For instance, a spectral excitation from the zero-point vibration on molecular ground PES only terminates at the vibrational levels of an excited electronic state with nuclear geometry similar to (or not too far away from) the ground equilibrium structure. This is also the reason why quantum states corresponding to molecular isomers, with dramatic geometric change from the most stable equilibrium structure, usually escape from spectroscopic observation, even though the isomers locate in the same PES.

Taking advantage of this vibrational overlap, spectral complexity can be reduced effectively by selecting a particular vibrational level as the initial state involved in a transition. For example, in our recent spectroscopic experiments of jet-cooled polyatomic molecules where most of the prepared molecules lie initially on the zero-point vibration, we have demonstrated that vibrational patterns in the electronic transitions to high-lying valence/Rydberg states (typically with

Table 2. Quantum Numbers and Their Corresponding Selection Rules Resulting from the Conservation Laws in the Rotation of a Symmetric-top Molecule

Conservation laws	Quantum numbers	Selection rules	
Angular momentum	J (Total rotational angular momentum)	$\Delta J = 0, \pm 1$	(dipole transitions)
	K (Projected rotational angular momentum / Geometric symmetry)	$\Delta K = \begin{cases} 0 \\ \pm 1 \end{cases}$	(∥ band) (⊥ bands)
Parity	±	$+ \leftrightarrow -$	(dipole transitions)
Nuclear spin modification	I	$\Delta I = 0$	(ortho ↔ ortho, para ↔ para)

excitation energy of 6-12 eV) can be analyzed quite satisfactorily. In our studies, electronic assignments have been facilitated with theoretical (*ab initio* and density functional) calculations and Rydberg-series formulation. In particular, we have successfully applied calculated FCFs to assist vibrational assignment for experimental vibronic spectra. The theoretical derivation for calculating the FCFs of polyatomic molecules will be discussed in subsequent sections.

In this article, I will review the excited valence/Rydberg states and IEs of several polyatomic molecules/radicals that we studied recently in our laboratory by resonance enhanced multiphoton ionization (REMPI) spectroscopy. Since discussions of molecular Rydberg states[18-27] and REMPI spectroscopy[28-44] can be found in previous reviews and monographs, I will only focus on the molecules/radicals that we examined recently. Specifically, we have utilized two-photon resonant ionization (i.e., 2+1 REMPI, Fig. 2) spectroscopy to investigate vinyl chloride,[45-47] propyne,[48] and allyl radical,[49-50] and will show the novel spectroscopic information of these molecules/radicals that we obtained in our laboratory. In these studies, we have emphasized spectroscopic observations from the first excited electronic states to the first IE's of the molecules/radicals of interest. The spectroscopic studies of the excited valence/Rydberg states of these polyatomic molecules have helped us to illuminate the photodissociation pathways and to manifest the usually complicated chemical-reaction mechanisms due to the multidimensionality in polyatomic PES.

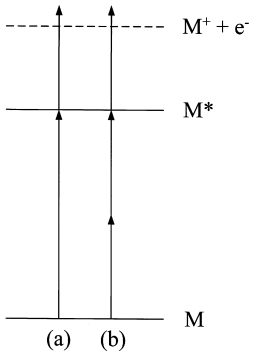

Fig. 2. Schematic diagram for the (a) 1+1′ and (b) 2+1 REMPI processes.

Compared with one-photon absorption spectroscopy, the advantages of applying a REMPI laser technique in studying polyatomic molecules/radicals are fourfold. First, monitoring an ion yield in spectroscopic experiments can technically be much more sensitive than a conventional photon detection. Second, the spectral resolution of tunable dye lasers is usually better than that of conventional VUV light source used in one-photon absorption spectroscopy. Detailed molecular structures can be resolved. Third, the REMPI spectroscopy can judiciously single out stable excited states leading to a simplified spectrum. Excited states with fast (pre)dissociation rates, compared to the ionization rate during a multiphoton process, can be excluded from REMPI spectrum unless very high laser power is used. Finally, the symmetries for excited states can be determined from polarization-ratio measurement in a two-photon transition (e.g., 2+1 REMPI). The polarization-ratio, Ω, is defined as the band-intensity ratio for circularly to linearly polarized radiations. According to two-photon theory, $\Omega < 3/2$ for the transitions from the totally symmetric ground state to the excited electronic states with full symmetry, and $\Omega = 3/2$ for those to the states of non-total symmetry.[28,51] With polarization-ratio measurement, the excited vibronic states with full symmetry can be discriminated unambiguously from the others.

The rest of this paper is organized as follows. An overview for the design of REMPI experiments is given in Section 2. Theoretical calculation for polyatomic FCFs will be described in Section 3. Next, results and discussion are presented in Section 4. Finally, conclusions are addressed in Section 5.

2. EXPERIMENTAL

REMPI Setup

The REMPI experiments were performed using a time-of-flight (TOF) mass spectrometer, and the details can be

found in several previous publications.[45-50,52,,53] A general schematic diagram for the REMPI/TOF experimental setup is shown in Fig. 3. Briefly, the molecules of interest were seeded in 2-3 atm helium to form a 0.1-10% mixture, which was expanded into the source vacuum chamber by a pulsed valve (General Valve, 0.5 mm or 0.8 mm orifice). The expanded molecular beam (~180 μs duration) was skimmed and injected to the TOF tube. A laser beam was tightly focused by a lens (f.l. = 15 cm or 25 cm) to reach a power intensity of ≥ 10 GW/cm^2, and aligned to intersect the molecular beam. The molecular cations produced via REMPI were repelled in an electric field with a direction perpendicular to both laser and molecular beams. These ions flew across the field-free TOF tube (80 cm) and were detected by a microsphere/microchannel plate (MSP/MCP, E1-Mu1). The time-sequence for the laser and molecular beams in the experiments was controlled by a digital pulse/delay generator (Stanford Research, DG535).

Preparation of Radicals

In radical experiments, the gaseous radicals were produced in the nozzle of a supersonic-jet expansion by the pyrolysis of precursor molecules. The nozzle consists of a resistant-heated molybdenum wire (Goodfellow, 0.127 mm dia.) and reaction-inert alumina tube (i.d. = 1.0 mm) with a heated zone of 10 mm extending to the orifice (Fig. 4). Owing to the low thermal conductivity of alumina material (κ = 30 Wm^{-1}K^{-1}), the molybdenum wire must be heated incandescently to reach the best temperature (estimated ≥ 1000 ℃) to produce radicals, and a glass tube was used to shield the sputtering molybdenum particles. The precursor (usually 1 Torr partial pressure) was seeded in 2-3 atm helium and expanded via a pulsed valve (General Valve, 0.8 mm orifice) at 30 Hz repetition rate. The molecular beam through a heated nozzle was flash-pyrolyzed (Fig. 4) and expanded into a vacuum chamber. The jet-expanded radical beam was skimmed and then injected into the ionization region of the TOF tube.

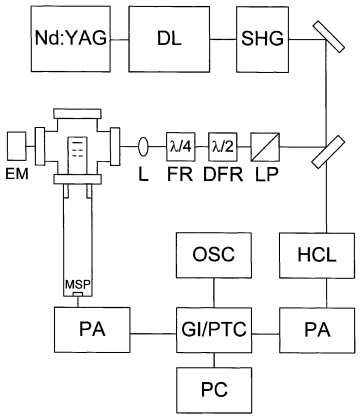

Fig. 3. Schematic diagram of the experimental setup for 2+1 REMPI spectroscopy: DL: dye laser; SHG: second harmonic generator; LP: linear polarizer; DFR: double Fresnel rhomb; FR: Fresnel rhomb; L: lens; EM: energy meter; MSP: microsphere plate; PA: preamplifier; GI: gated integrator; PTC: photon counter; OSC: oscilloscope; PC: personal computer; HCL: hollow cathode lamp.

Light Sources and Ion Detection

A tunable dye laser (Lambda Physik, Scanmate 2E) pumped by the frequency-doubled (532 nm) or -tripled (355 nm) output of a Nd:YAG laser (Spectra Physics, GCR-190) was operated at 30 Hz with pulse duration of ~7 ns. The spectral resolution of grating scan is ~0.2 cm^{-1}. Because of the predissociative nature of the high-lying valence/Rydberg states of polyatomic molecules and partly due to the medium sizes of the molecules under our present study,[45-50] molecular rotational features were usually not resolved in our REMPI spectra, even if an etalon scan (resolution ~0.03 cm^{-1}) of the dye laser was applied. The double-frequency output of the dye laser is typically 0.1-10 mJ/pulse generated via KDP and BBO crystals. The detected signal from the MSP/MCP was amplified by a preamplifier (EG&G, VT120) and sent to a digital oscilloscope (LeCroy, 9344) and a personal computer. In the REMPI experiment, the amplified signal was processed in a gated integrator (Stanford Research, SR250) and then an A/D converter. A computer program was developed to control the dye laser and to acquire the digitized data from the A/D converter.

REMPI spectra were obtained by gating at a selected mass and monitoring the ion yield as a function of excitation laser frequency. For each step in the frequency scan, signal was averaged for 60-100 laser shots to reduce the noise caused by laser fluctuation. An optogalvanic hollow-cathode lamp filled with neon (Hamamatsu, L233-13NB) was employed simultaneously in the spectral scan for frequency calibration (Fig. 3). The accuracy of this calibration is within 2

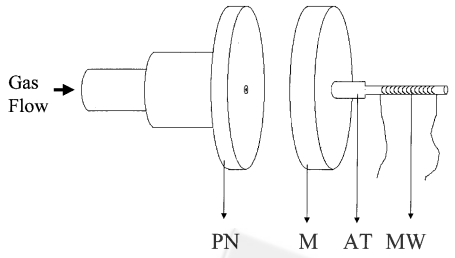

Fig. 4. The pulsed nozzle with heat zone. PN: pulsed nozzle, M: mount, AT: alumina tube, MW: molybdenum wire.

cm^{-1}; frequency difference could be measured with an estimated precision of ± 0.5 cm^{-1}. In some experiments (e.g., for propyne[48]), a daughter ion channel ($C_3H_3^+$, m/z = 39) was used to obtain the REMPI spectra as it typically gave stronger signals than the parent ion ($C_3H_4^+$, m/z = 40). Nevertheless, the spectra obtained from these two (daughter and parent) channels were proved, with much care, to be the same within experimental uncertainty. In the case when the parent-ion signal was too weak, a photon counter (Stanford Research, SR400) was used to replace the gated integrator.

Polarization Ratios

For polarization-ratio measurement (Fig. 3), a linear polarizer was used to form linearly polarized laser radiation. The linearly polarized laser then passes through a double Fresnel rhomb (CVI, FR-2-UV) and a Fresnel rhomb (CVI, FR-4-UV), functioning respectively as half-wave and quarter-wave retarders. By rotating the double Fresnel rhomb, the polarization vector of the laser is set at 0°/45° with respect to the optical axis of the Fresnel rhomb to form linearly/circularly polarized radiation. The polarization-ratio measurement can be conducted in two ways. One is to measure the band-intensity ratios from the REMPI spectra obtained separately with linear and circular polarizations. Due to laser fluctuation and energy decay during the laser frequency scan, the polarization-ratio for a particular transition can optionally be measured with laser frequency fixed at the top of the transition. The measured integrated-TOF-intensities were taken with linear and circular lasers separately and were averaged for 1000 laser shots for each measurement. As such, the energy fluctuation of the two polarized lasers can be reduced within 0.5%. The results from both methods agree with each other; the latter, nevertheless, is more precise. The laser energy can also be measured concurrently using an energy meter (Fig. 3) for a power-dependence study.

3. THEORETICAL CALCULATION

Franck-Condon Factors

The theoretical derivation for calculating the FCFs of polyatomic molecules has been discussed in several previous publications.[54-56] Even though the calculations have been simplified by taking a harmonic-oscillator approximation for each normal vibration, the derived formula for the FCFs are mathematically lengthy as can be found in Refs. 54 and 55. To briefly summarize the calculations of the FCFs of polyatomics, the following procedures were included.

(a) Optimize the geometries of the ground and excited electronic states.
(b) Calculate the vibrational frequencies and the normal modes for the two electronic states.
(c) Calculate the displacements of the oscillators between ground and excited electronic states.
(d) Compute the vibrational overlap integrals, FCFs and positions of the peaks in spectra.

As demonstrated in the previous studies of ethylene,[54,55] vinyl radical,[57,58] acetone,[59-60] vinyl chloride,[46,47] and allyl radical,[49,50] we have successfully applied the calculated FCFs to assist spectroscopic assignment for experimental vibronic spectra. In our previous studies, we have primarily focused on the calculation that the potential-energy curves for the vibrational normal-modes are displaced, but not distorted. Accordingly, the FCF, $|I_{a0bv}|^2$, for a transition from the zero-point vibration of ground state a to the v^{th} vibration of excited electronic state b is given by

$$|I_{a0bv}|^2 = \frac{S^v e^{-s}}{v!} \quad \text{and} \quad S = \frac{\omega(\Delta Q)^2}{2\hbar} \tag{1}$$

where S is a Huang-Rhys factor, ΔQ is the displacement in terms of normal coordinates, ω is the vibrational frequency of the corresponding normal mode, and $h = 2\pi\hbar$ is the Planck constant. The maximum FCF is found for v = [S], the integer part of S. This means that the larger the displacement of the normal mode, the greater v for the most intense vibronic transition. On the other hand, with a small displacement, the spectral intensities along the vibrational progression are of exponential-decay character.[56]

Generally, we employed *ab initio* methods and density functional theory for the computations. In some calculations for molecular excited electronic states,[48] we realized that the time-dependent density functional theory (TDDFT) method[61,62] is a better choice for theoretical studies of Rydberg states, especially for the high-lying ones. For multi-reference configuration interaction (MRCI)[63,64] or complete active space SCF (CASSCF)[65,66] methods, more and more vacant orbitals have to be included into the active space for the calculations of high-lying Rydberg states, and computational convergence is usually a difficult technical problem.

The TDDFT method,[61,62] however, is unable to optimize the geometry of excited states at the present time. Since Rydberg state geometry is often similar to the structure of cations, we have usually taken cationic geometry and vibrational frequencies as those of the Rydberg states. We have optimized the ground-state geometries for both neutral molecule/radical of interest and its corresponding cation using a commercial computational package, such as Gaussian 94.[67] The normal modes and frequencies obtained from these cal-

culations were then employed for calculating FCFs.

Unlike conventional assignment for polyatomic vibronic spectra where seeking vibrational progressions is the major procedure in spectral analysis, the calculated FCFs in our studies have assisted us in not only locating the positions of vibronic transitions, but also in providing intensity ratios to identify each vibronic band. Based on these calculated spectral patterns, line-by-line comparison with experimental spectra is generally feasible. In particular, the vibrational intensity-ratio in an electronic transition obtained from the calculated FCFs is so crucial that it often makes a spectroscopic analysis possible.

Excited Electronic States

As mentioned before, *ab initio* calculations of the (adiabatic and vertical) excitation energies, geometries, and transition dipoles for electronically excited polyatomics have made a significant improvement to the spectral assignments in modern molecular electronic spectroscopy. Benefits from the advanced development in theoretical (*ab initio* and density functional) calculations,[10-14] molecular electronic states can nowadays be identified quite effectively. Taking one of our recent studies on vinyl chloride as an example, the broad bands of the molecule at 45000-60000 cm^{-1}, previously attributed to a $\pi^* \leftarrow \pi$ transition [The corresponding excited state is represented as (π, π^*) in this article.], have been calculated by *ab initio* methods and reassigned as due to two *triplet* ← *singlet* and five *singlet* ← *singlet* transitions.[47] The details for the spectral analysis will be discussed in the subsequent Sec. 4.1.

4. RESULTS AND DISCUSSION

4.1. REMPI Spectra and Theoretical Calculations

Vinyl chloride

We have spectroscopically examined the vinyl chloride

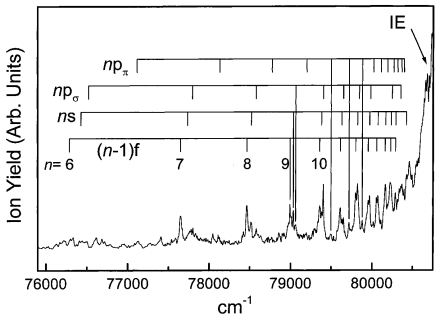

Fig. 5. Composite 2 + 1 REMPI spectrum of vinyl chloride at 76000-80600 cm^{-1}.

Table 3. Peak Positions (cm^{-1}), Ionization Energies (IE), and Quantum Defects (δ) for the Four Observed Rydberg Series of Vinyl Chloride[a,b]

n	(π, ns)	(π, np_σ)	(π, np_π)	(π, nf)
3			63043	
4	68682	69156	71764	73639
5	73870	74200	75278	76301
6	76410	76496	77112	77646
7	(77732)	77790	78128	78464
8	78518	78575	(78770)	78992
9	79032	79060	(79195)	79356
10	79379	79403	79498	79611
11	79632	79650	79720	79800
12	79823	(79844)	79881	79951
13	79970	(79983)	80017	80056
14	80073		80109	80160
15	(80167)		80190	80229
16	(80235)	(80248)	(80265)	80288
17	(80293)		80313	
18		(80351)	80364	
19			80394	
20	(80421)			
IE	80731 ± 7	80722 ± 16	80722 ± 4	80727 ± 8
δ	0.983 ± 0.003	0.915 ± 0.007	0.507 ± 0.001	0.055 ± 0.007

[a]The values in parentheses belong to weak or congested bands.

[b]The listed IE for each Rydberg series is extrapolated from all of the observed Rydberg states. If only the higher-lying Rydberg states ($n \geq 6$) are included, IE = 80720 ± 6 cm^{-1} results from fitting to the Rydberg formula (see text).

(VC, C_2H_3Cl) molecule from its first excited electronic state (~6 eV) to the first ionization energy (IE, ~10 eV). In the higher energy region of 76000-85000 cm^{-1} (Fig. 5), we have investigated VC using 2+1 REMPI spectroscopy,[45] and have been able to identify four Rydberg series as due to the transitions of *n*s, *n*p$_\sigma$, *n*p$_\pi$, and *n*f $\leftarrow \pi$, where the corresponding excited states are denoted by (π, *n*s), (π, *n*p$_\sigma$), (π, *n*p$_\pi$), and (π, *n*f), respectively (Table 3). In fitting to the Rydberg-formula, all of the four series converge to the same IE limit, 80720 ± 6 cm^{-1}, corresponding to the ground state of VC cation, and will be discussed further in Sec. 4.2.

In 60000-76000 cm^{-1} (Fig. 6), the transitions to the Rydberg states of *n*s, *n*p$_\sigma$, *n*p$_\pi$, *n*d, *n*f (*n* = 3, 4) $\leftarrow \pi$ and 3s $\leftarrow$ n_{Cl} are responsible for the observed REMPI spectra of VC.[46] The complex vibrational structures for the observed transitions are successfully identified with the aid of calculated FCFs. Ultimately, we have been able to assign the vibronic spectra peak by peak, e.g., the 3p$_\pi \leftarrow \pi$ transitions shown in Fig. 7 and Table 4. More than 100 vibronic transitions of VC at 62000-78000 cm^{-1} have been successfully identified (Tables 4 and 5).[46] The spectroscopic analysis for the excited vibronic states have provided detailed information to the photo-excitation mechanisms in this molecule. For instance,

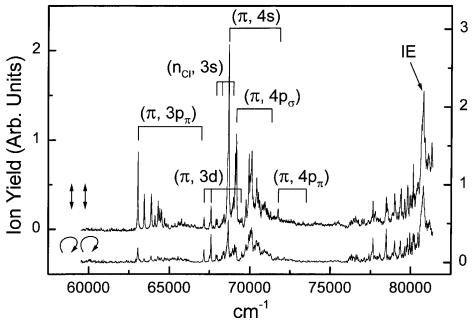

Fig. 6. Composite 2+1 REMPI spectra of vinyl chloride at 60000-80600 cm^{-1}.

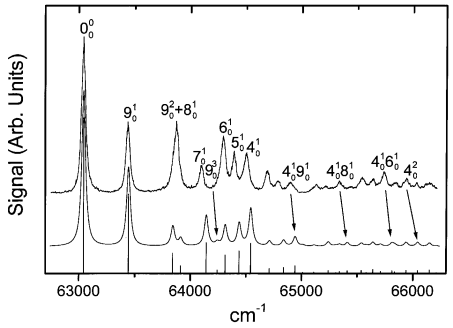

Fig. 7. Franck-Condon factors (vertical lines at the bottom), calculated vibronic spectra (middle trace), and the observed 3p$_\pi \leftarrow \pi$ transitions (upper trace) of vinyl chloride.

Radloff and coworkers recently measured the internal-conversion rate of 60 ± 20 fs in VC upon excitation at 155 nm (64516 cm^{-1}).[68] From our spectroscopic study, we realize that

Table 4. Peak Positions (cm^{-1}), Assignment, and the Calculated Franck-Condon Factors (FCF) for the 3p$_\pi \leftarrow \pi$ Transitions of Vinyl Chloride

Peak	Assignment	FCF
62338	8_1^0	
62644	9_1^0	
63043	0_0^0	0.11643
63436	9_0^1	0.05908
63863	9_0^2	0.01499
	$+ 8_0^1$	0.00568
64096	7_0^1	0.02289
64199	9_0^3	0.00253
64292	$8_0^1 9_0^1$	0.00165
	$+ 6_0^1$	0.01368
64391	5_0^1	0.01678
64500	$7_0^1 9_0^1$	0.00574
	$+ 4_0^1$	0.02246
64690	$6_0^1 9_0^1$	0.00372
64786	$5_0^1 9_0^1$	0.00444
64897	$7_0^1 8_0^1 + (7_0^1 9_0^2)$	(0.00146)
	$+ 4_0^1 9_0^1$	0.00566
65129	$6_0^1 8_0^1 + (6_0^1 9_0^2)$	(0.00094)
65213	$5_0^1 8_0^1 + (5_0^1 9_0^2)$	(0.00113)
	$+ 7_0^2$	0.00225
65338	$4_0^1 8_0^1 + (4_0^1 9_0^2)$	(0.00144)
	$+ 6_0^1 7_0^1$	0.00196
65442	$5_0^1 7_0^1$	0.00235
65542	6_0^2	0.00080
	$+ 4_0^1 7_0^1$	0.00299
65635	$5_0^1 6_0^1$	0.00152
65740	$6_0^1 7_0^1 9_0^1$	0.00060
	$+ 4_0^1 6_0^1$	0.00193
	$+ 5_0^2$	0.00121
65837	$4_0^1 5_0^1$	0.00231
65936	$6_0^2 9_0^1 + (4_0^2)$	(0.00217)
66030	$5_0^1 6_0^1 9_0^1 + (3_0^1)$	(0.00255)
66142	$4_0^1 6_0^1 9_0^1$	0.00059
	1_0^1	0.10727
66235	$4_0^1 5_0^1 9_0^1$	0.00071
66355	$6_0^2 8_0^1$	
66440	$5_0^1 6_0^1 8_0^1 + (3_0^1 9_0^1)$	(0.00076)
66561	$4_0^1 6_0^1 8_0^1$	
66681	$4_0^1 5_0^1 8_0^1$	
66786	6_0^3	
66882	$5_0^1 6_0^2$	
66983	$4_0^1 6_0^2$	

$(\pi, 3p_\pi)4^1_0$, $(\pi, 3p_\pi)7^1_0 9^1_0$,and some other nearby states (Fig. 7 and Table 4) are involved in the initially prepared wave-packet, depending on the bandwidth of the excitation laser. Namely, when the VC molecule is excited at 155 nm, a π-electron is promoted to the $3p_\pi$ orbital and the vibrational energy is deposited to the C=C (ν_4: C=C stretching), CH_2 (ν_7: CH_2 rocking), and C–Cl (ν_9: C–Cl deforming) chemical bonds. Upon the excitation of VC at 157 nm (63694 cm^{-1}) with a F_2 excimer laser, it is the Rydberg states in the vicinity of $(\pi, 3p_\pi)9^1_0$, 9^2_0 and 8^1_0 (ν_8: C–Cl stretching; Fig. 7 and Table 4) that initiate the subsequent serial photodissociation processes.

In 45000-60000 cm^{-1}, we have calculated the vibronic spectrum of VC for the transitions from ground state to the lowest-lying five excited states,[47] and found that the major contributions in this spectral region are from the $\tilde{A}(1^1A'') \leftarrow \tilde{X}(1^1A')$ (i.e., $3s/\sigma^* \leftarrow \pi$) and $\tilde{C}(2^1A') \leftarrow \tilde{X}(1^1A')$ (i.e., π^*

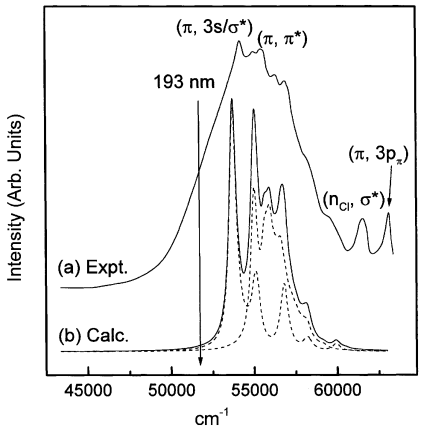

Fig. 8. (a) Experimental absorption spectrum (upper) of vinyl chloride (taken from Ref. 69). (b) calculated vibronic spectrum (lower). The dashed lines represent the spectra of the $3s/\sigma^* \leftarrow \pi$ and $\pi^* \leftarrow \pi$ transitions, respectively.

Table 5. Assignment for the Observed Peaks (cm^{-1}) in the 2 + 1 REMPI Spectra of Vinyl Chloride from 67100 to 77510 cm^{-1}

Peak	Assignment	Peak	Assignment	Peak	Assignment
67148	$(\pi, 3d)\,0^0_0$	70585	$(\pi, 4p_\sigma)\,4^1_0$	74418	$(\pi, 4d)\,7^1_0$
67525	$(\pi, 3d)\,9^1_0$	70746	$(\pi, 4s)\,6^1_0 8^1_0$	74476	$(\pi, 4f)\,8^1_0$
67595	$(\pi, 3d')\,0^0_0$	70837	$(\pi, 4s)\,5^1_0 8^1_0$	74550	$(\pi, 4f')\,8^1_0$
67907	$(n_{Cl}, 3s)\,0^0_0$	70940	$(\pi, 4s)\,4^1_0 8^1_0$	74715	$(\pi, 4p_\pi)8^1_0$
67974	$(\pi, 3d)\,8^1_0$	71096	$(\pi, 4s)\,4^1_0 7^1_0$	74798	$(\pi, 4f')\,7^1_0$
67991	$(\pi, 3d')\,9^1_0$	71153	$(\pi, 4s)\,6^2_0$	74847	$(\pi, 4d)\,4^1_0$
68207	$(\pi, 3d)\,7^1_0$	71259	$(\pi, 4s)\,5^1_0 6^1_0$	74911	$(\pi, 5s)\,7^1_0$
68270	$(n_{Cl}, 3s)\,9^1_0$	71339	$(\pi, 4p_\sigma)\,7^2_0$	74958	$(\pi, 4f')\,6^1_0$
68368	$(\pi, 3d)\,6^1_0$	71417	$(\pi, 4s)\,4^1_0 5^1_0$	75278	$(\pi, 5p_\pi)\,0^0_0$
68416	$(\pi, 3d')\,8^1_0$	71516	$(\pi, 4s)\,4^2_0$	75555	$(\pi, 5p_\sigma)\,5^1_0$
68609	$(n_{Cl^*}, 3s)\,0^0_0$	71612	$(\pi, 4p_\sigma)\,4^1_0 7^1_0$	75679	$(\pi, 5p_\pi)\,9^1_0$
68682	$(\pi, 4s)\,0^0_0$	71662	$(\pi, 4s)\,5^1_0 6^1_0 9^1_0$	75722	$(\pi, 5s)\,4^1_0 9^1_0$
68882	$(n_{Cl}, 3s)\,7^1_0$	71764	$(\pi, 4p_\pi)\,0^0_0$	76301	$(\pi, 5f)\,0^0_0$
68965	$(n_{Cl^*}, 3s)\,9^1_0$	71835	$(\pi, 4p_\sigma)\,4^1_0 6^1_0$	76335	$(\pi, 5p_\pi)\,7^1_0$
68987	$(\pi, 3d)\,4^1_0 9^1_0$	72160	$(\pi, 4p_\pi)9^1_0$	76410	$(\pi, 6s)\,0^0_0$
69077	$(\pi, 4s)\,9^1_0$	72590	$(\pi, 4p_\pi)8^1_0$	76496	$(\pi, 6p_\sigma)\,0^0_0$
69156	$(\pi, 4p_\sigma)0^0_0$	72830	$(\pi, 4p_\pi)7^1_0$	76574	$(\pi, 5p_\pi)\,6^1_0$
69315	$(\pi, 3d)\,4^1_0$	72971	$(\pi, 4p_\pi)6^1_0$	76600	$(\pi, 5p_\pi)\,5^1_0$
69436	$(\pi, 3d')\,8^1_0$	73114	$(\pi, 4p_\pi)5^1_0$	76682	$(\pi, 5f)\,9^1_0$
69503	$(\pi, 4s)\,8^1_0$	73217	$(\pi, 4p_\pi)\,4^1_0$	76739	$(\pi, 5p_\pi)\,4^1_0$
69550	$(\pi, 4p_\sigma)9^1_0$	73372	$(\pi, 4d)\,0^0_0$	76827	$(\pi, 6s)\,9^1_0$
69738	$(\pi, 4s)\,7^1_0$	73504	$(\pi, 4d')\,0^0_0$	76981	$(\pi, 5p_\pi)\,6^1_0 9^1_0$
69921	$(\pi, 4s)\,6^1_0$	73639	$(\pi, 4f)\,0^0_0$	77112	$(\pi, 6p_\pi)\,0^0_0$
69968	$(\pi, 4p_\sigma)\,8^1_0$	73724	$(\pi, 4f')\,0^0_0$	77241	$(\pi, 6s)\,8^1_0$
70025	$(\pi, 4s)\,5^1_0$	73795	$(\pi, 4p_\pi)6^1_0 8^1_0$	77319	$(\pi, 6p_\sigma)\,8^1_0$
70099	$(\pi, 4s)\,4^1_0$	73870	$(\pi, 5s)\,0^0_0$	77357	$(\pi, 5f)\,7^1_0$
70192	$(\pi, 4p_\sigma)7^1_0$	74034	$(\pi, 4f)\,9^1_0$	77504	$(\pi, 6p_\pi)\,9^1_0$
70402	$(\pi, 4p_\sigma)6^1_0$	74090	$(\pi, 4f')\,9^1_0$		
70513	$(\pi, 4p_\sigma)5^1_0$	74200	$(\pi, 5p_\sigma)\,0^0_0$		

Table 6. Band Position, Polarization-Ratio, Vibronic Symmetry, State Assignment, Vibrational Frequency and Quantum Defect of Vibronically Excited Propyne Studied by 2+1 REMPI Spectroscopy and Theoretical Calculation

Experimental results							Theoretical results				
One-photon absorption[a]		REMPI					TDDFT and *ab initio*				
Band position[b]	Assignment[c]	Band position	Ω	Vibronic symetry[d]	Assignment	Vibration/ δ	Assignment	TDDFT[e]	Osc. str.[f]	MRCI[f]	Osc. str.[f]
58007 (7.19)	(π, π*)						1^1E (π, 3s)	6.84	0.02	6.97	0.078
59459 (7.37)	(π, π*)						1^1A_2 (π, π*)	6.77	0.0	7.45	0.0
60612 (7.51)	(π, π*)						2^1E (π, π*)	6.89	0.0	7.53	0.001
63411 (7.86)	?						3^1E (π, $3p_z$)	7.79	0.06	7.64	0.0006
64178	?										
64323	$3R'-(\nu_9)_0$										
64928	3R'	64927 (8.05)	0.19	A_1	(π, $3p_{x,y}$) (A_1) 0^0_0	δ = 0.58	2^1A_1 (π, $3p_{x,y}$)	7.95	0.07	7.91	0.062
65242	$3R'+\nu_{10}$										
		65681	1.21	E	(π, $3p_{x,y}$) (A_1) 9^1_0	ν_9 = 754					
65887	$3R'+\nu_5$	65878	0.33	A_1	(π, $3p_{x,y}$) (A_1) 5^1_0	ν_5 = 951					
66484	$3R'+\nu_7$										
		66157 (8.20)	1.18	E	(π, $3p_{x,y}$) (E) 0^0_0	δ = 0.49	4^1E (π, $3p_{x,y}$)	8.02	0.0		
							2^1A_2 (π, $3p_{x,y}$)	8.03	0.0		
66879	$3R'+\nu_3$	66896	0.44	A_1	(π, $3p_{x,y}$) (A_1) 3^1_0	ν_3 = 1969					
		67681	0.66	A_1	(π, $3p_{x,y}$) (A_1) 2^1_0	ν_2 = 2754					
		67865	0.47	A_1	(π, $3p_{x,y}$) (A_1) $3^1_0 5^1_0$						
68138	3R"	68123(8.45)	1.24	E	(π, $3d_{z^2}$) (E) 0^0_0 / (π, $3p_{x,y}$) (E) 3^1_0	δ=0.34/ ν_3 = 1966	5^1E (π, $3d_z2$)	8.30	0.03		
68864	$3R'+2\nu_3$	68828	0.58	A_1	(π, $3p_{x,y}$) (A_1) 3^2_0						
69622	$3R"+\nu_7$										
70098	$3R"+\nu_3$										
70719	$3R'+3\nu_3$										
							3^1A_1 (π, $3d_{xz,yz}$)	8.69	0.04		
							3^1A_2(π, $3d_z2\text{-}_y2_{,xy}$)	8.70	0.0		
							6^1E (π, $3d_z2\text{-}_y2_{,xy}$)	8.71	0.003		
							4^1A_1(π, $3d_z2\text{-}_y2_{,xy}$)	8.73	0.03		
		70897 (8.79)	1.08	A"(E)	(π, 4s) (A") 0^0_0	δ = 1.06	7^1E (π, 4s)	8.74	0.0		
71195	4R	71203 (8.82)	0.26	A'(E)	(π, 4s) (A') 0^0_0	δ = 1.03					
							8^1E (π, $3d_{xz,yz}$)	8.78	0.01		
							4^1A_2(π, $3d_{xz,yz}$)	8.78	0.0		
72082	$3R"+2\nu_3$										
72727	$3R'+4\nu_3$										
73179	$4R+\nu_3$	73192	0.18	A'(E)	(π, 4s) (A') 3^1_0	ν_3 = 1989					
74292 (9.21)	4R'						9^1E (π, $4p_z$)	9.09	0.01		
							5^1A_1(π, $4p_{x,y}$)	9.11	0.05		
							10^1E (π, $4p_{x,y}$)	9.12	0.0		
							5^1A_2(π, $4p_{x,y}$)	9.13	0.0		
75171 (9.32)	$4R+2\nu_3$										
75558 (9.37)	4R"						11^1E (π, $4d_z2$)	9.25	0.01		
75727 (9.39)	$4R'+\nu_7$										
							6^1A_1(π, $4d_{xy,xz,yz}$)	9.34	0.05		
							12^1E (π, $4d_x2\text{-}_y2$)	9.36	0.0		
							6^1A_2(π, $4d_{xy,xz,yz}$)	9.36	0.0		
							13^1E (π, $4d_{xy,xz,yz}$)	9.37	0.0		
							7^1A_1(π, $4d_x2\text{-}_y2_{,xy}$)	9.38	0.03		
							14^1E (π, $4d_{xy,yz}$)	9.40	0.0		
		76061 (9.43)	1.06	E	(π, 4p) 3^1_0 ?						
76219	$4R'+\nu_3$	76270 (9.46)	0.72	A_1	(π, 4p) 3^1_0 ?						
76768	5R	76718	1.19	A"(E)	(π, 5s) (A") 0^0_0	δ = 1.01					
		76862	0.26	A'(E)	(π, 5s) (A') 0^0_0	δ = 0.97					

77107	$4R+3\nu_3$					
77550	$4R"+\nu_3$					
77945	5R'					
78163	$4R'+2\nu_3$					
78591	5R"					
78751	$5R+\nu_3$	78724	1.22	A"(E)	(π, 5s) (A") 3^1_0	ν_3 = 2000
		78851	0.69	A'(E)	(π, 5s) (A') 3^1_0	ν_3 = 1989
		79177	1.04	A"(E)	(π, 6s) (A") 0^0_0	δ = 1.03
79276	6R	79318	0.6	A'(E)	(π, 6s) (A') 0^0_0	δ = 0.95
79913	6R'					
80163	6R"					
		80542	1.11	A"(E)	(π, 7s) (A") 0^0_0	δ = 1.03
80591	7R	80627	0.84	A'(E)	(π, 7s) (A') 0^0_0	δ = 0.95
80881	7R'					
81147	7R"					
		81357		A"(E)	(π, 8s) (A") 0^0_0	δ = 1.04
		81412		A'(E)	(π, 8s) (A') 0^0_0	δ = 0.96
81607	8R'					
81700[#]	8R"					
		81880		A"(E)	(π, 9s) (A") 0^0_0	δ = 1.07
		81931		A'(E)	(π, 9s) (A') 0^0_0	δ = 0.95
82030[#]	9R'					
82140[#]	9R"					
		82282		A'/E	(π, 10s) 0^0_0	δ = 0.96
82420[#]	10R"					
		82541		A'/E	(π, 11s) 0^0_0	δ = 0.94
		82729		A'/E	(π, 12s) 0^0_0	δ = 0.93
		82866		A'/E	(π, 13s) 0^0_0	δ = 0.98

[a] One-photon VUV absorption spectra taken from Ref. 81 (denoted by #) and Ref. 82.
[b] Units in cm^{-1}. The number in parenthesis is of eV unit to compare with the calculation.
[c] R, R' and R" are s, p and d Rydberg series, respectively.
[d] A_1 and E are symmetry representations of a C_{3v} group; A' and A" belong to C_s. A'(E) and A"(E) represent the symmetry correlation of E in C_{3v} to A' and A" in C_s.
[e] Units in eV. The calculated values are vertical excitation energies.
[f] The oscillator strength is for one-photon transition.

$\leftarrow \pi$) transitions as shown in Fig. 8. In this study, two spin-forbidden transitions of $\tilde{b}(1^3A") \leftarrow \tilde{X}(1^1A')$ and $\tilde{c}(2^3A") \leftarrow \tilde{X}(1^1A')$ are calculated to locate in 45000-54000 cm^{-1}, and could be responsible for the observed one-photon absorption spectrum in this region[69] due to an intensity borrowing caused by spin-orbit coupling of the Cl atom. Based on the calculation, we argued that upon excitation of VC at 193 nm (51800 cm^{-1}) the $\tilde{b}(1^3A")$ or $\tilde{c}(2^3A")$ excited state, instead of the previously assigned (π, π^*) [i.e., $\tilde{C}(2^1A')$], is initially prepared prior to subsequent photodissociation processes (Fig. 8).

Photodissociation of VC excited at the convenient wavelength of 193 nm with an ArF laser has been heavily explored in the past decades.[70-80] It was generally conceived that the (π, π^*) state of VC was excited in the photo-absorption at 193 nm.[79] In the wake of the $\pi^* \leftarrow \pi$ excitation, various dissociation channels were taken to the (π, σ^*_{C-Cl}) excited-state or the ground-state PES, probably via internal conversions.[79] This kind of argument was usually concluded from measuring the velocity and angular distributions of photofragments, but the correlated excited states involved in the photodissociation pathways were rarely verified theoretically. Based on our calculation, the (π, 3s/σ^*_{C-Cl}) and (π, π^*) states are too high to be reached with 193 nm excitation (Fig. 8), and we argue that the $\tilde{b}(1^3A")$ and $\tilde{c}(2^3A")$ excited states could be responsible for the excitation of VC at 193 nm.[47] In future, reexamination of the photodissociation of VC at 193 nm is suggested taking these triplet states into account.

Propyne

The vibronic spectra of jet-cooled propyne (CH_3CCH) at 64500–85000 cm^{-1} have been observed using 2+1 REMPI spectroscopy (Figs. 9-12).[48] The (π, 4-13s), (π, 3-4p) and (π, $3d_{z^2}$) Rydberg states of propyne have been identified (Table 6). The symmetries of the excited vibronic states have been

determined directly from polarization-ratio experiments applying linearly and circularly polarized lasers. The vertical excitation energies of (π, π*), (π, 3-4s), (π, 3-4p) and (π, 3-4d) states, calculated with time-dependent density functional theory (TDDFT) and *ab initio* methods, have assisted our assignments for the observed electronic transitions in REMPI spectra (Table 6). Compared with one-photon absorption spectrum of propyne, the absence of (π, π*), (π, *n*p) ($n \geq 4$) and (π, *n*d) ($n \geq 3$, except (π, $3d_{z^2}$)) Rydberg states in the observed REMPI spectra suggests a strong predissociation character for these states.[48]

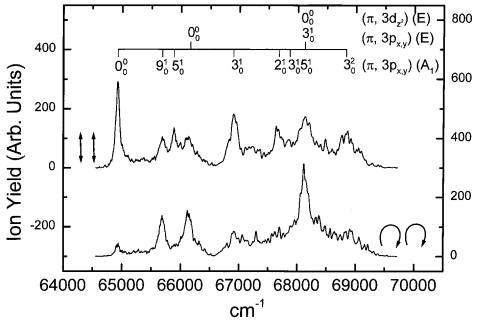

Fig. 9. Polarization dependence for the 2+1 REMPI spectra of propyne at 64000-70000 cm^{-1}. The left and right scales indicate linearly (upper trace) and circularly (lower trace) polarized excitations, respectively.

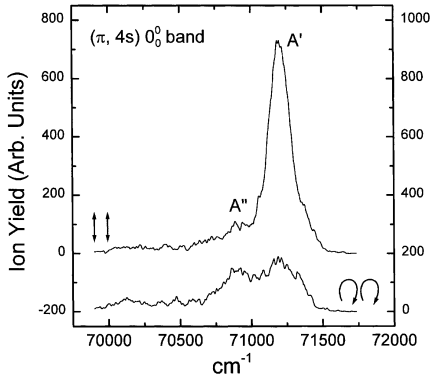

Fig. 10. Polarization dependence for the 2+1 REMPI spectra of propyne at 70000-72000 cm^{-1}.

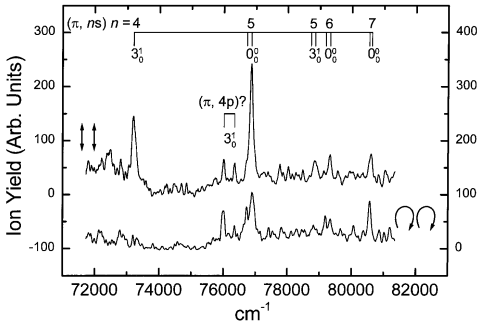

Fig. 11. Polarization dependence for the 2+1 REMPI spectra of propyne at 72000-81000 cm^{-1}.

In the study of the Rydberg states of propyne by REMPI spectroscopy, clear doublet splittings/broadenings have been observed in the origin bands of the (π, 4-9s) Rydberg series (Fig. 10–12). The splittings, 306 cm^{-1} at (π, 4s), decrease with increasing *n*. The doublet components have very different polarization ratios (Figs. 10-12 and Table 6). The splitting in the (π, *n*s) Rydberg series can be interpreted as follows. If the propyne molecule is of C_{3v} structure, the (π, *n*s) Rydberg states should have E symmetry corresponding to the promotion of a π-electron (E symmetry) to the s Rydberg orbital (A_1). However, earlier calculations of the (π, 3s) (E) state of propyne showed that its geometry is significantly distorted with respect to C_{3v} symmetry.[83] The optimized geometry for this state has one C-H bond length different from the other two in the methyl group, and is only of C_s symmetry. Therefore, the (π, 3s) (E) electronic state splits into two components, A′ and A″, and the energy splitting between them is sizable. The splittings/ broadenings caused by the reduced molecular symmetry from C_{3v} to C_s have now been observed in the (π, 4-9s) Rydberg states of propyne.

Moreover, it is noted from the calculation that the large distortion of geometry in the (π, 3s) Rydberg state of propyne is, in part, due to the contribution of (π, π*) mixed in the (π, 3s) wavefunction.[83] In higher Rydberg states, this contribution will be diminishing and then disappear, which agrees very well with the gradual decrease of the observed splittings with increasing *n*. Although our calculations with density functional theory show that propyne cation has C_s symmetry, the barrier to methyl rotation in the cation is very low, only a few cm^{-1}, lower than the zero-point energy of the methyl tor-

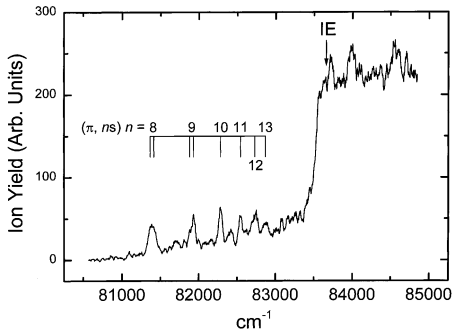

Fig. 12. 2+1 REMPI spectrum of propyne at 81000-84500 cm^{-1}. The arrow marks the adiabatic IE (83625 cm^{-1}) of propyne extrapolated from the (π, 6-13s) Rydberg series.

sion.[48] Thus, the propyne cation has an effective C_{3v} geometry. This further explains the observation that the splitting nearly disappears for high (π, *n*s) Rydberg states, because the A′ and A" components (C_s symmetry) of the (π, *n*s) Rydberg states will merge to the same E level (C_{3v} symmetry) in the cationic state. This convergence of the (π, *n*s) Rydberg series of propyne will be discussed more in Sec. 4.2.

Within the C_s point group, the observed doublets in the (π, *n*s) Rydberg states are of A′ and A" symmetries which correlate to the E symmetry in C_{3v}. For a two-photon process in the propyne molecule of C_s symmetry, the polarization-ratios are $\Omega = 3/2$ for A" states and $\Omega < 3/2$ for A′.[28] This is evidenced by the peaks at 70897 cm^{-1} and 71203 cm^{-1} (Fig. 10) of the origin bands of (π, 4s) (A") and (π, 4s) (A′), respectively. Similar splittings/broadenings due to the A′ and A" components have also been observed in the (π, 5-9s) Rydberg states (Figs. 11 and 12). With linear polarization, spectral intensities for the A′ components of the (π, 4–7s) Rydberg states are much stronger than those of A" (Figs. 10-12). Based on this observation, we represent the symmetry for the observed, but unresolved doublets, (π, 10-13s) Rydberg states of propyne as A′ in C_s or E in C_{3v} (Table 6).

Allyl radical

In the studies of allyl-h_5 (CH_2CHCH_2) and allyl-d_5 (CD_2CDCD_2) radicals, we have produced these radicals by the flash-pyrolysis of allyl iodide (CH_2CHCH_2I) and deuterated allyl bromide (CD_2CDCD_2Br), respectively. Before our 2+1 REMPI spectroscopic studies on the Rydberg states of allyl-h_5 and allyl-d_5 radicals,[49,50] only the $\tilde{A}^2B_1$, $\tilde{B}^2A_1$, $\tilde{C}^2B_1$, and $\tilde{D}^2B_2$ electronic states with excitation energies less than 6 eV had been investigated.[84-94] The 2+1 REMPI experiment in our laboratory has been conducted to observe the high-lying Rydberg states of allyl-h_5 and allyl-d_5 radicals at 6.0-8.2 eV. Through spectroscopic analysis, the transitions corresponding to the excitation of a nonbonding electron to the *n*s Rydberg orbitals, denoted by *n*s ← nb, are responsible for the observed 2+1 REMPI spectra. Totally, we have observed nine (nb, 4-12s) Rydberg states of allyl-h_5 radical and seven (nb, 4-10s) states of allyl-d_5 radical (Figs. 13-15 and Table 7).

Depicted in Figs. 13b and 13d are the theoretical spectra (only including FCFs) of allyl-h_5 and allyl-d_5 radicals, respectively, for the vibronic transitions from the electronic ground to an "ionlike" Rydberg state.[49,50] The geometries and normal-mode frequencies obtained at the (U)MP2/6-311++G(d, p) level using the Gaussian 94 package[67] were employed for calculating FCFs. The calculated FCFs are quite similar for both allyl-h_5 and allyl-d_5 radicals, except that the C_3-stretching (ν_6) is more active in allyl-h_5 while the CH_2-rocking (ν_5) is more visible in allyl-d_5. The ∠CCC-bending (ν_7) is the most active vibrational mode among others, because of the relatively pronounced change in the ∠CCC coordinate from 124.3° in ally radical to 117.4° in allyl cation. The calculated spectral intensities along the prominent bending (ν_7) progression have shown a typical exponential-decay character (Figs. 13b and 13d), representing that the displacement in the ∠CCC coordinate between the ground and "ionlike" Rydberg states is not that large.

Figs. 13a and 13b show a comparison between the observed (nb, 4s) spectrum and the calculated FCFs of allyl-h_5, where peaks at 54137 cm^{-1} (7_0^1) and 54563 cm^{-1} (7_0^2) are the ∠CCC-bending vibrational progression. Peaks at 54742 cm^{-1} (6_0^1) and 55175 cm^{-1} ($6_0^1 7_0^1$) are C_3 stretching (1034 cm^{-1}) and stretching-bending combination (1467 cm^{-1}) modes, respectively. The 53288 cm^{-1} peak, 420 cm^{-1} red shift to the 4s band origin, is due to a hot-band transition from the ground ν_7 state. For allyl-d_5, Figs. 13c and 13d show the calculated FCFs and the observed (nb, 4s) spectrum. Good agreement in peak positions for the 0_0^0, 7_0^1, 7_0^2, 7_0^3, 5_0^1 and $5_0^1 7_0^1$ bands between calculation and experiment is clearly seen.

The calculated spectral intensities for the 0_0^0 and 7_0^1 bands of allyl-h_5, however, are reverse to the observed ones (Figs. 13a and 13b). The situation is similar to that in allyl-d_5 (Figs. 13c and 13d). One of the possible explanations as to

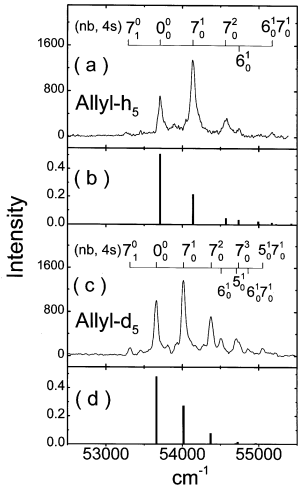

Fig. 13. (a) The 2 + 1 REMPI spectrum of allyl-h5 radical at 52500-55500 cm^{-1}. (b) The calculated Franck-Condon factors for the vibronic transitions of allyl-h_5 radical from the electronic ground to an "ionlike" Rydberg state. (c) The 2 + 1 REMPI spectrum of allyl-d_5 radical. (d) The calculated Franck-Condon factors of allyl-d_5 radical.

Table 7. Vibronic Band Positions and Spectral Assignment for Allyl Radicals Studied by 2 + 1 REMPI Spectroscopy[a]

	REMPI[b]					Absorption[c]	
	Allyl-h_5		Allyl-d_5			Allyl-h_5	Allyl-d_5
Vibronic assignment	Band position	Vibrational frequency[d]	Band position	Vibrational frequency[d]	Isotopic shift[e]	TPE / OPE	TPE / OPE
Ground 0_0^0	0		0				
Ground 7_0^1	427[f]	427	345[f]	345			
Ground 7_0^2	856[f]	856					
(nb, 3s)0_0^0	40057[f]		40096[f]		+39		
(nb, 3s)7_0^1	40450[f]	393	40415[f]	319			
(nb, 3s)7_0^2			40734[f]	638			
						48970 / 24485 s	49490 / 24745 s
						49210 / 24605 w	49924 / 24962 w
						49688 / 24844 m	51136 / 25568 m
						50786 / 25393 m	51452 / 25726 m
						50980 / 25490 m	51800 / 25900 w
						51452 / 25726 m	53036 / 26518 w
(nb, 3d)	52114						
						52826 / 26413 w	
(nb, 4s)7_1^0	53288	-420	53312	-349		53290 / 26645 m	
							53418 / 26709 m
	53454		53459				
(nb, 4s)0_0^0	53708		53661		-47	53704 / 26852 w	
							53748 / 26874 w
	53898		53812				
(nb, 4s)7_0^1	54137	429	54017	356			
							54214 / 27107 w
(nb, 4s)7_0^2	54563	855	54379	718			
(nb, 4s)6_0^-	54742	1034	54509	848			
							54570 / 27285 w
(nb, 4s)5_0^1			54708	1047			
(nb, 4s)7_0^3			54736	1075			
(nb, 4s)$6_0^1 7_0^1$	55175	1467	54862	1201			
							54930 / 27465 w
(nb, 4s)$5_0^1 7_0^1$			55054	1393			
(nb, 5s)0_0^0	58979		58926		-53		
(nb, 5s)7_0^1	59415	436	59283	357			
(nb, 6s)7_1^0			60940	-344			
(nb, 6s)0_0^0	61337		61284		-53		
(nb, 6s)7_0^1	61776	439	61647	363			
(nb, 6s)7_0^2	62215	878	62003	719			
(nb, 7s)0_0^0	62620		62567		-53		
			62622				
(nb, 7s)7_0^1	63069	449	62926	359			
(nb, 7s)7_0^2			63292	725			
(nb, 8s)0_0^0	63398		63340		-58		
(nb, 8s)7_0^1	63844	446	63702	362			
(nb, 9s)0_0^0	63914		63840		-74		
(nb, 10s)0_0^0	64266		64203		-63		
	64300						
(nb, 11s)0_0^0	64511						
(nb, 12s)0_0^0	64696						

[a] Unit: cm^{-1}. [b] Refs. 49 and 50. [c] Ref. 84. TPE: two-photon energy. OPE: one-photon energy. [d] Relative to the origin band.
[e] The value of allyl-d_5 with respect to that of allyl-h_5. [f] Refs. 90-100.

why the (nb, 4s) 0_0^0 of allyl-h_5 (at 53708 cm^{-1}) is weaker than the (nb, 4s) 7_0^1 is that the first laser photon in the 2+1 REMPI process is accidentally resonant with one of the predissociative vibrational levels in the $\tilde{A}^2B_1$ state of allyl-h_5 at 26852 cm^{-1} (two-photon energy of 53704 cm^{-1}, Table 7) observed by Currie and Ramsay.[84] Because of the predissociative $\tilde{A}^2B_1$ state, the 2+1 REMPI intensity for the (nb, 4s) 0_0^0 band of allyl-h_5 would otherwise be stronger than it is observed. The reverse intensity as due to accidental resonance, however, is ruled out by the same two-photon transitions of the (nb, 4s) 0_0^0 and 7_0^1 bands in allyl-d_5. While there is no accidental resonance in allyl-d_5 (Table 7), the observed intensities for the (nb, 4s) 0_0^0 and 7_0^1 bands of allyl-d_5 are still reverse to the calculation (Figs. 13c and 13d).

Therefore, the weaker band intensity of (nb, 4s) 0_0^0, compared with that of (nb, 4s) 7_0^1, indicates that the actual displacement along the ∠CCC coordinate between the ground and the (nb, 4s) Rydberg state is larger than the calculated. The deviation could be due to considerable difference in the structures between the actual (nb, 4s) Rydberg state and the assumed allyl cation used in the calculation. Besides, the (nb, 4s) Rydberg state is likely perturbed. The term value of the (nb, 4s) 0_0^0 state deviates severely from the Rydberg formula for the (nb, *n*s) Rydberg series of allyl radical, and will be discussed in the subsequent section.

Also in Fig. 13c, the relatively stronger peak at 54509 cm^{-1} (848 cm^{-1} relative to the (nb, 4s) 0_0^0) and the rather weak one at 54862 cm^{-1} (1201 cm^{-1}) could be assigned as the (nb, 4s) 6_0^1 and $6_0^1 7_0^1$ bands, respectively, based on the excellent frequency coincidence with the calculated ν_6 = 846 cm^{-1} and ν_7 = 355 cm^{-1} in allyl-d_5 Rydberg state (Table 1 of Ref. 49). According to the calculated FCFs of allyl-d_5 (Fig. 13d), both 6_0^1 and $6_0^1 7_0^1$ bands, however, are too weak to appear in spectrum. This intensity discrepancy between observation and calculation might again originate from the fact that the geometry of the (nb, 4s) Rydberg state differs considerably from that of allyl cation used in the FCF calculation. Alternatively, if the (nb, 4s) Rydberg state was subject to perturbation, as will be discussed in Sec. 4.2, these weak signals could as well stem from the interaction with some nearby unidentified dark states.

Unlike the (nb, 4s) state where the 0_0^0 band and several vibrational modes have been observed (Fig. 13), higher-lying (nb, *n*s) ($n \geq 5$) Rydberg states usually show up with the 0_0^0 band alone, or are accompanied at most by the active 7_0^1 and 7_0^2 vibrations (Figs. 14 and 15). The vibrational frequency of the ∠CCC-bending (ν_7) mode increases, roughly with a monotonic manner (Table 7), from 427 cm^{-1} in the ground state[95-100] to ~446 cm^{-1} in the (nb, 8s) Rydberg state, except the much lower 393 cm^{-1} in the (nb, 3s) ($\tilde{B}^2A_1$) state, where a strong interaction among the $\tilde{B}^2A_1$, $\tilde{C}^2B_1$ and $\tilde{D}^2B_2$ states was reported.[91-94] Partly due to the decreasing signal-to-noise ratio, the shoulders on the 0_0^0 bands of (nb, 8s) and (nb, 10s) (Fig. 15) were not assigned.

For the (nb, 5s) state of allyl-d_5, only 0_0^0 and 7_0^1 bands were observed (Fig. 14b). Fig. 15 shows a the (nb, 6-10s) Rydberg series of the allyl-d_5 radical. While the shoulder on the (nb, 7s) 0_0^0 band is still without assignment, prominent bending (ν_7) progressions in the (nb, 6-8s) states are easily recognized. The vibrational frequency of the most active ν_7 mode also increases from 345 cm^{-1} in the ground state[95-100] to ~360 cm^{-1} in the higher-lying (nb, *n*s) Rydberg states (Table 7), again, except the low 319 cm^{-1} at (nb, 3s).

The spectral intensities along the bending (ν_7) progres-

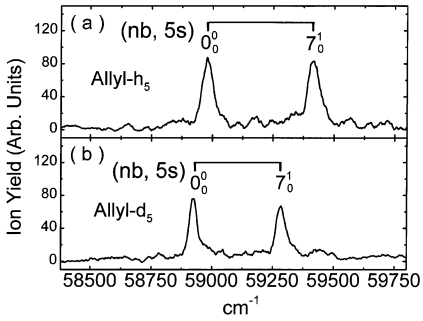

Fig. 14. The observed (nb, 5s) 0_0^0 and 7_0^1 bands in the 2 + 1 REMPI spectra of (a) allyl-h_5 and (b) allyl-d_5 radicals at 58500-59750 cm^{-1}.

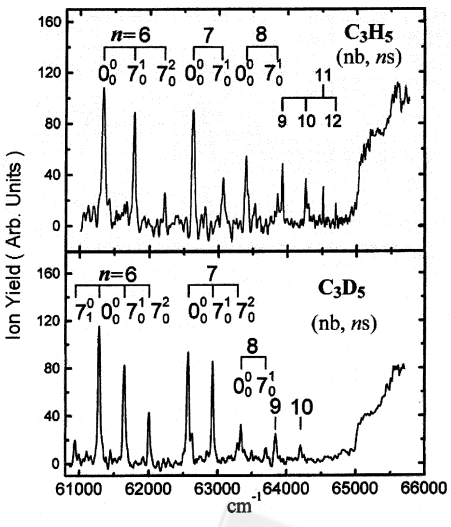

Fig. 15. The observed 2 + 1 REMPI spectra of allyl-h_5 and allyl-d_5 radicals at 61000-65750 cm^{-1}.

sions in the (nb, 6-8s) Rydberg states of allyl-h_5 and allyl-d_5 (Fig. 15) have shown a similar exponential-decay character with the predicted (Fig. 13b and 13d). The structures of the (nb, 6-8s) Rydberg states are accordingly little displaced from the ground equilibrium geometry in the ∠CCC coordinate. Although the signal-to-noise ratios for the (nb, *n*s) (n > 8) transitions become smaller and the bending (ν_7) progression is no longer visible (Fig. 15), the strongest origin bands in the observed (nb, 9-12s) Rydberg states agree very well with the calculation. The consistence in the spectral patterns between theory and experiment, especially for the high-lying (nb, *n*s) ($n \geq 6$) Rydberg states, also justifies the assumption used in our FCF calculation that the structures and vibrations of high-lying Rydberg states are similar to those of allyl cation.

4.2. Ionization Energy

Taking the Rydberg series observed in REMPI spectra, we have fitted the origin bands (0_0^0) of the Rydberg states to Rydberg formula

$$\nu = IE - \frac{R}{(n-\delta)^2} \quad (2)$$

where ν is the transition frequency in cm^{-1}, IE is the first ionization energy, R is the Rydberg constant, n is a principal quantum number, and δ is the corresponding quantum defect. The IE and δ values of the molecule of interest can be obtained from the fitting. The resulting δ value can further assist in labeling the Rydberg series (e.g., s, p, d, f etc.). For hydrocarbon-related molecules, the typical values for quantum defects are $\delta \sim 1$ for s orbitals, $\delta \sim 0.5$ for p, $\delta \leq 0.3$ for d, and $\delta < 0.1$ for f.

Vinyl chloride

As discussed in Sec. 4.1, we have observed four series of excited vibronic states of vinyl chloride (VC) at 63000-80500 cm^{-1} by 2+1 REMPI spectroscopy (Table 3).[45,46] Without rotationally resolved band-origins in our observed vibronic spectra, the transition frequency at half width at half maximum (HWHM) of the spectral line-profile for each 0_0^0 band has been taken as the term value of the corresponding Rydberg state. The observed Rydberg states are fitted to the Rydberg formula [Eq.(2)], in which R = 109736.3588 cm^{-1} is the Rydberg constant taking the mass of VC into account and the other terms are previously defined. All of the four series, (π, *n*s), (π, *n*p$_\sigma$), (π, *n*p$_\pi$) and (π, *n*f) (n = 3-20), converge to the same IE limit, 80722 ± 16 cm^{-1}, corresponding to the ground state of VC cation. Due to the probable penetration to the molecular core, low-lying Rydberg states usually cause sizeable deviation from the Rydberg formula and should be excluded from the fitting in order to get an accurate IE.[24,45,46,48] Accordingly, IE = 80720 ± 6 cm^{-1} is extrapolated from the higher-lying states of the (π, *n*s), (π, *n*p$_\sigma$), (π, *n*p$_\pi$) and (π, *n*f) (n = 6-20) Rydberg series. The IE = 80720 ± 6 cm^{-1} agrees very well with the IE values determined from other methods.[101-103]

The assigned four Rydberg series of VC as due to the transitions of *n*s, *n*p$_\sigma$, *n*p$_\pi$, and *n*f ← π are justified by their δ values. In Table 3, the quantum defects of 0.983 ± 0.003, 0.507 ± 0.001 and 0.055 ± 0.007 resulting from the fittings are in good agreement with the generally accepted δ values for molecular s, p$_\pi$ and f Rydberg series. The δ = 0.915 ± 0.007 value of the in-plane (π, *n*p$_\sigma$) Rydberg series is more pronounced than δ = 0.507 ± 0.001 of the out-of-plane (π, *n*p$_\pi$). The δ = 0.915 ± 0.007 of (π, *n*p$_\sigma$) in VC is also slightly larger than those for the (π, 3p$_y$) (δ = 0.76) and (π, 3p$_z$) (δ = 0.72) Rydberg states of ethylene (C_2H_4).[104] (By definition, the molecular plane of C_2H_3Cl or C_2H_4 is designated as yz-plane. The *n*p$_x$ thus corresponds to an *n*p$_\pi$ orbital, and the *n*p$_y$ and *n*p$_z$ correlate with *n*p$_\sigma$ orbitals.) Unfortunately, the (π, *n*p$_y$) and (π, *n*p$_z$) (n > 3) Rydberg states of ethylene and other chloroethylenes have not been reported to date for comparison. Compared with ethylene, the presence of the Cl atom in VC is responsible for the larger δ value in the (π, *n*p$_\sigma$) Rydberg series. A bigger atom in the molecular core will cause more steric hindrance to Rydberg electrons when they travel nearby the molecular core, hence rendering larger deviation (i.e., pronounced δ) from a hydrogen-atom model. Therefore, the Cl atom, a third-row element of VC, is responsible for the larger quantum defect rather than the C (second-row) and H (first-row) atoms. It is difficult, however, to distinguish the contribution of (π, *n*p$_y$) from that of (π, *n*p$_z$) in the present study. Consequently, this series is denoted as the (π, *n*p$_\sigma$) of VC in this study.

Propyne

We have fitted the observed (π, *n*s) Rydberg series of propyne (Table 6) to the Rydberg formula [Eq. (2)], where R = 109735.8235 cm^{-1} is the Rydberg constant taking the mass of propyne into account. The fitting of (π, 6-13s) (A′) Rydberg series of propyne to the Rydberg formula renders IE = 83625 ± 2 cm^{-1} (10.3682 ± 0.0002 eV) and δ = 0.95. This adiabatic IE of propyne, 10.3682 ± 0.0002 eV, determined from our REMPI data is in excellent agreement with the most recent experimental value of 10.369 ± 0.007 eV.[82] We have also found that the (π, 6-9s) (A") series converges to a limit at 83613 ± 9 cm^{-1}, which is slightly lower than 83625 ± 2 cm^{-1} of

the (π, *n*s) (A′) series and will be discussed later. It is noted that the δ values for all A′ components in the (π, 4-9s) Rydberg series are slightly smaller than those for the A" components. In Table 6, we have calculated the δ value for the origin band of each observed Rydberg state using the Rydberg formula [Eq. (2)] and IE = 83625 cm^{-1}. It is rewarding to see δ ~0.3 for (π, 3d), δ ~0.5 for (π, 3p) and δ ~1.0 for the (π, *n*s) Rydberg states of propyne, which justify the assignment for the observed Rydberg series.

The assignment for the observed (π, *n*s) Rydberg series of propyne (Table 6), rather than (π, *n*p), (π, *n*d) or (π, *n*f), can be further confirmed by the following examinations. The average quantum defects δ = 0.97 and 1.04, respectively for the assigned (π, *n*s) (A′) and (π, *n*s) (A") series (Table 6), are typical for s Rydberg orbitals. Should the Rydberg series of (π, *n*s) (A′) be attributed to (π, (*n*-1)p/d/f) or (π, (*n*+1)p/d/f), the fitted δ = -0.03 or 1.97 would be quite unacceptable in a usual sense. For (π, *n*s) (A"), a small δ = 0.04 would be found, if the series of (π, *n*s) were assigned to (π, (*n*-1)f); (π, (*n*-1)d) is ruled out due to δ ~0.3 for the (π, *n*d) states in this molecule as shown earlier. The assignment for (π, (*n*-1)f), however, is not allowed, because the (π, 4s) (A") state would then be replaced by a nonexistent (π, 3f).

It is interesting to ask whether the (π, *n*s) (A′) and (π, *n*s) (A") Rydberg series converge to the same IE. As discussed earlier, if the propyne cation is of C_s symmetry, the (π, *n*s) (A′) and (π, *n*s) (A") series would converge to different ionization limits which should appear in the ZEKE spectrum of propyne. Conversely, the two series converge to the same IE corresponding to the $^2E_{1/2}$ spin-orbit state of the C_{3v} propyne cation.[105] The ZEKE spectrum of propyne observed by Matsui et al. indicates that only the origin band, a transition from the neutral ground state to the ionic ground state, shows up which led them to conclude that the structure of the cation is very similar to that of the neutral.[106] The doublet in the ZEKE spectrum can be well fitted by assuming a spin-orbit constant of 30 cm^{-1} for the cation and an identical structure (C_{3v}) for both the cation and the neutral. In this study, we found that the (π, 6-9s) (A") series converges to a limit at 83613 ± 9 cm^{-1}, which is slightly lower than 83625 ± 2 cm^{-1} of the (π, 6-13s) (A′) series. However, both values lie within the bandwidth of the lower spin-orbit doublet component of the propyne cation observed in the ZEKE spectrum of propyne.[106] Consequently, we conclude that the two series converge to the same IE.

Allyl radical

The observed 0_0^0 bands of the (nb, 4-12s) Rydberg series for allyl-h_5 and (nb, 4-10s) for allyl-d_5, are listed in Table 7. As before, the term values of the observed (nb, *n*s) Rydberg states have been fitted to the Rydberg formula of Eq. (2) with R_H = 109735.8601 cm^{-1} and R_D = 109736.0095 cm^{-1} being the Rydberg constants for allyl-h_5 and allyl-d_5, respectively. Listed in Table 8 are several fittings, with various combinations of the (nb, *n*s) Rydberg states, to the Rydberg formula for the allyl radical. In all of the fittings, the quantum defects ($\delta \approx 0.92$) are close to a typical value (~1.0) for the s Rydberg orbitals of a hydrocarbon molecule.

Allyl-h_5

Neglecting the (nb, 3s) and (nb, 4s) states of allyl-h_5 in the fitting, the extrapolated IE values from various sets of (nb, *n*s) ($n \geq 5$) states are well converged to the range of 65590–65598 cm^{-1} (Table 8). It is noteworthy that the inclusion of (nb, 4s) state always causes very large error-bars in the extrapolated IE values. If only the (nb, 4s) state is excluded, IE = 65595 ± 2 cm^{-1} results from the fitting where even the lowest (nb, 3s) state is included. These outcomes indicate that the (nb, 4s) state deviates severely from the Rydberg formula and is likely perturbed.

In addition to the measurement uncertainty in the experimental transition frequency (estimated ±5 cm^{-1}), the extrapo-

Table 8. Ionization-energy and Quantum-defect Fittings of the (nb, *n*s) Rydberg Series of Allyl Radical to the Rydberg Formula

Allyl-h_5			Allyl-d_5		
Quantum number *n*	Ionization energy IE (cm^{-1})	Quantum defect δ	Quantum number *n*	Ionization energy IE (cm^{-1})	Quantum defect δ
3-12	65576 ± 32	0.929 ± 0.004	3-10	65505 ± 45	0.924 ± 0.005
4-12	65622 ± 16	0.960 ± 0.006	4-10	65572 ± 23	0.960 ± 0.007
3, 5-12	65595 ± 2	0.927 ± 0.001	3, 5-10	65533 ± 3	0.923 ± 0.001
5-12	65595 ± 2	0.927 ± 0.001	5-10	65533 ± 5	0.923 ± 0.003
6-12	65593 ± 2	0.923 ± 0.003	6-10	65526 ± 5	0.913 ± 0.005
7-12	65594 ± 3	0.926 ± 0.005	7-10	65524 ± 9	0.911 ± 0.014
8-12	65594 ± 4	0.926 ± 0.012			

lated IE of allyl-h_5 locates at 65590–65598 cm^{-1} for various fittings with (nb, *n*s) ($n \geq 5$) Rydberg states (Table 8). For the sake of caution, we adjusted the error limit of the extrapolated IE value upwards to include all of these uncertainties. As a consequence, IE = 65594 ± 9 cm^{-1} for allyl-h_5 radical is obtained from the REMPI data. Without rotationally resolved band-origins, the term values for the (nb, *n*s) Rydberg states, again, were taken from the transition frequencies at HWHM of the (nb, *n*s) 0_0^0 band-profiles. Judging from the rotationally resolved infrared spectra of ν_1 and ν_{13} bands,[107,108] and the partially rotation-resolved 1+1 MPI vibronic spectra of allyl radical,[93] an energy difference between the band-origin and the point at HWHM of band-profile is estimated ≤ 7 cm^{-1}, which should be well covered in the quoted error limit (± 9 cm^{-1}).

The IE = 65594 ± 9 cm^{-1} (8.133 ± 0.001 eV) obtained from our experiment agrees with those values determined previously from other methods, such as photoelectron spectroscopy (8.13 ± 0.02 eV[109] or 8.15 ± 0.02 eV[110]) and electron impact measurement (8.18 ± 0.07 eV).[111] In particular, the currently obtained IE = 8.133 ± 0.001 eV is very close to the IE = 8.13 ± 0.02 eV determined by Houle and Beauchamp.[109] Despite a relatively low resolution, the spectral pattern of ν_7 vibrational progression in the one-photon absorption photoelectron spectra observed by Houle and Beauchamp,[109] with ~420 cm^{-1} spacings and an exponential-decay intensity ratio along the progression, is in excellent agreement with our calculated FCF of allyl-h_5 radical (Fig. 13b).

Recently, an IE value of 65762 ± 5 cm^{-1} for allyl-h_5 radical has been obtained by Gilbert et al. from a 1+1′ ZEKE experiment,[112] where the vibrational levels of the $\tilde{B}^2A_1$ or $\tilde{C}^2B_1$ excited electronic state were taken as intermediates in the 1+1′ double-resonance processes. The IE = 65762 ± 5 cm^{-1}, however, is 168 cm^{-1} blue-shifted to the IE = 65594 ± 9 cm^{-1} determined from our REMPI data. According to *ab initio* calculation,[49] the allyl-h_5 cation is a bent structure with ∠CCC = 117.4°. The most soft vibrational mode in allyl-h_5 cation is a CH_2 symmetric-twisting with ν_{12} ~260 cm^{-1}.[49,112] The difference of 168 cm^{-1} in the IE between REMPI and ZEKE cannot match with any vibrational mode of allyl-h_5 cation. Further investigation into the difference between these IE values is called for in the future.

Allyl-d_5

For allyl-d_5, the fittings to the Rydberg formula with various (nb, *n*s) Rydberg states are also tabulated in Table 8. Similar to allyl-h_5, the inclusion of the (nb, 4s) Rydberg state of allyl-d_5 causes large error-bars in the IE . As discussed in the preceding section for allyl-h_5, neglecting the (nb, 3s) and (nb, 4s) states in the fitting and taking all of the uncertainties into account, IE = 65527 ± 16 cm^{-1} (8.124 ± 0.002 eV) is obtained for allyl-d_5 radical.

In our REMPI study, we found that the observed (nb, *n*s) Rydberg series of allyl radical have a well convergent trend. The isotopic shifts in the (nb, 4-10s) 0_0^0 bands between allyl-h_5 and allyl-d_5 are quite parallel (Table 7) with an average 57 ± 8 cm^{-1} red-shift by allyl-d_5, except the (nb, 3s) ($\tilde{B}^2A_1$) state with a 39 cm^{-1} blue-shift.[90-94]

5. CONCLUSIONS

We have observed and calculated the valence/Rydberg states of vinyl chloride, propyne, and allyl radical by 2+1 REMPI spectroscopy and theoretical (*ab initio* and density functional) methods. In the study of vinyl chloride, we have been able to identify the vibronic transitions, essentially line by line, from its first excited electronic state to the first ionization energy at 45000-85000 cm^{-1}. For propyne, we have observed clear A′ and A" doublet splittings/broadenings in the (π, 4-13s) Rydberg series, due to a reduced molecular symmetry (from C_{3v} in the ground state to C_s in the s Rydberg orbitals) and the contamination of (π, π*) wavefunction in the (π, *n*s) Rydberg states. For allyl radicals, we have successfully observed and spectroscopically analyzed nine (nb, 4-12s) Rydberg states of allyl-h_5 and seven (nb, 4-10s) states of allyl-d_5 for the first time.

The ionization energies of vinyl chloride, propyne, allyl-h_5 radical and allyl-d_5 radical have been determined, respectively, 80720 ± 6 cm^{-1} (10.0080 ± 0.0007 eV), 83625 ± 2 cm^{-1} (10.3682 ± 0.0002 eV), 65594 ± 9 cm^{-1} (8.133 ± 0.001 eV) and 65527 ± 16 cm^{-1} (8.124 ± 0.002 eV) from the extrapolations of the observed Rydberg series.

ACKNOWLEDGEMENTS

I am indebted to the former and present members in my group, Dr. J.-L. Chang, Dr. R. Li, Mr. J.-C. Shieh, Mr. J.-C. Wu, Mr. C.-W. Liang, Mr. C.-C. Chen, Ms. C.-Y. Wei and Ms. H.-C. Wu, for their tremendous contributions to the work presented in this article. I also wish to thank Dr. A. M. Mebel and Professor N. C. Handy for their calculations of the propyne molecule and to express my appreciation of the collaboration with Professor S. H. Lin in various research subjects over the past years. This work is supported by National Science Council of ROC (NSC-90-2113-M-001-037) and dedicated to celebration of the 70th anniversary of the Chemical Society located in Taipei.

Received July 15, 2002.

Key Words

Rydberg states; Ionization energy; Hhydrocarbon-related molecules; Radicals; Two-photon spectroscopy.

REFERENCES

1. Wodtke, A. M.; Lee, Y. T. *Molecular Photodissociation Dynamics*, Royal Society of Chemistry: London, 1987.
2. Michl, J.; Bona i -Koutecký, V. *Electronic Aspects of Organic Photochemistry*, John Wiley & Sons: New York, 1990.
3. Schinke, R. *Photodissociation Dynamics*, Cambridge University Press: Cambridge, 1993.
4. Yung, Y. L.; DeMore, W. B. *Photochemistry of Planetary Atmospheres*, Oxford University Press: New York, 1997.
5. Minkin, V. I.; Simkin, B. Ya.; Minyaev, R. M. *Quantum Chemistry of Organic Compounds*, Springer-Verlag: Berlin, 1990.
6. Albright, T. A.; Burdett, J. K.; Whangbo, M.-H. *Orbital Interactions in Chemistry*, John Wiley & Sons: New York, 1985.
7. Hirota, E. High-Resolution Spectroscopy of Transient Molecules, Springer-Verlag: Berlin, 1985.
8. Fischer, G. *Vibronic Coupling*, Academic Press: London, 1984.
9. Yang, C. N. *Science* **1958**, *127*, 565.
10. Schleyer, P. V. R. *Encyclopedia of Computational Chemistry*, John Wiley & Sons: New York, 1998.
11. Hehre, W. H.; Radom, L.; Schleyer, P. v. R.; Pople, J. A. *Ab Initio Molecular Orbital Theory*, John Wiley & Sons: New York, 1986.
12. Hohenberg, P.; Kohn, W. *Phys. Rev.* **1964**, *136*, B864.
13. Kohn, W.; Sham, L. J. *Phys. Rev*. **1965**, *140*, A1133.
14. Parr, R. G.; Yang, W. *Density-Functional Theory of Atoms and Molecules*, Oxford Science: Oxford, 1989.
15. Lu, K. T.; McGlynn, S. P.; Findley, G. L.; Huebner, R. H. *Elements of Quantum Defect Theory: A Unified Theory of Rydberg and Autoionizing States*, D. Reidel Publishing: Dordrecht, 1985.
16. Greene, C. H.; Jungen, Ch. *Adv. At. Mol. Phys.* **1985**, *21*, 51.
17. Garcia-Sucre, M.; Raseev, G.; Ross, S. C. *Half Collision Resonance Phenomena in Molecules*, AIP Conference Proceedings , American Institute of Physics: New York, 1991.
18. Debree, E.; Delange, C. A.; Westwood, N. P. C. *Phys. Rev. A* **1992**, *46*, 5653.
19. Shang, Q. Y.; Brnstein, E. R. *Chem. Rev.* **1994**, *94*, 2015.
20. Kim, S. H.; Mazur, E. *Phys. Rev. A* **1995**, *52*, 992.
21. Clark, W.; Greene, C. H., Miecznik, G. *Phys. Rev*. *A* **1996**, *53*, 2248.
22. Woutersen, S.; Milan, J.B.; Buma, W. J.; deLange, C. A. *Phys. Rev. A* **1996**, *54*, 5126.
23. Reichle, R.; Mistrik, I.; Muller, U.; Helm, H. *Phys. Rev. A* **1999**, *60*, 3929.
24. Duncan, A. B. F. *Rydberg Series in Atoms and Molecules*, Academic, New York, 1971.
25. Stebbings, R. F.; Dunning, F. B. *Rydberg States of Atoms and Molecules*, Cambridge, New York: Cambridge University Press, 1983.
26. Gallagher, T. F. *Rydberg Atoms*, Cambridge University Press, 1994.
27. Child, M. S. *Molecular Rydberg Dynamics*, Imperial College Press: London, 1997.
28. Lin, S. H.; Fujimura, Y.; Neusser, H. J.; Schlag, E. W. *Multiphoton Spectroscopy of Molecules*, Academic Press: Orlando, 1984.
29. Letokhov, V. S. *Laser Photoionization Spectroscopy*, Academic: Orlando, 1987.
30. Miller, C. M.; Parks, J. E. *Resonance Ionization Spectroscopy*, IOP: Bristol, 1992.
31. Vertes, A.; Adams, R. G. F. *Lasers and Mass Spectroscopy*, John Wiley & Sons: New York, 1993.
32. Hurst, G. S.; Payne, M. G.; Kramer, S. D.; Young, J. P. *Rev. Mod. Phys.* **1979**, *51*, 767.
33. Johnson, P. M. *Acc. Chem. Res.* **1980**, *13*, 20.
34. Johnson, P. M.; Otis, C. E. *Ann. Rev. Phys. Chem.* **1981**, *32*, 139.
35. Schlag, E. W.; Neusser, H. J. *Acc. Chem. Res.* **1983**, *16*, 355.
36. Powis, I., *Molecular Photodissociation Dynamics*, Ashfold, M. N. R.; Baggott, J. E., Eds.; Royal Society of Chem: London, 1987.
37. Pratt, S. T.; Dehmer, P. M.; Dehmer, J. L. *Adv. Multi-Photon Processes Spectrosc.* **1988**, *4*, 69.
38. Compton, R. N.; Miller, J. C. *Laser Applications in Physical Chemistry*, Evans, D. K., Ed.; Marcel Dekker: New York, 1989.
39. Goodman, L.; Philis, J. Applied Laser Spectroscopy: Techniques, Instrumentaion, and Applications, Andrews, D. L., Ed.; VCH: New York, 1992.
40. Anderson, S. L. *Adv. Chem. Phys.* **1992**, *82*, 177.
41. Mark, S.; Glenewinkel-Meyer, Th.; Gerlich, D. *Int. Rev. Phys. Chem.* **1996**, *15*, 283.
42. Ashfold, M. N. R. *Nonlinear Spectroscopy and Molecular Structure Determination*, Field, R. W., Ed.; Blackwell: Oxford, 127, 1998.
43. Dessent, C. E. H.; Mueller-Dethlefs, K. *Chem. Rev.* **2000**, *100*, 3999.

44. Dedonder-Lardeux, C.; Gregoire, G.; Jouvet, C.; Martrenchard, S.; Solgadi, D. *Chem. Rev.* **2000**, *100*, 4023.
45. Chang, J.-L.; Shieh, J.-C.; Wu, J.-C.; Li, R.; Chen, Y.-T. *Chem. Phys. Lett.* **2000**, *325*, 369.
46. Chang, J.-L.; Li, R.; Wu, J.-C.; Shieh, J.-C.; Chen, Y.-T. *J. Chem. Phys.* **2001**, *115*, 5925.
47. Chang, J.-L.; Chen, Y.-T. *J. Chem. Phys.* **2002**, *116*, 7518.
48. Shieh, J.-C.; Chang, J.-L.; Wu, J.-C.; Li, R.; Mebel, A. M.; Handy, N. C.; Chen, Y.-T. *J. Chem. Phys.* **2000**, *112*, 7384.
49. Wu, J.-C.; Li, R.; Chang, J.-L.; Chen, Y.-T. *J. Chem. Phys.* **2000**, *113*, 7286.
50. Liang, C.-W.; Chen, C.-C.; Wei C.-Y.; Chen, Y.-T. *J. Chem. Phys.* **2002**, *116*, 4162.
51. Chen, K.; Yeung, E. S.; *J. Chem. Phys.* **1978**, *69*, 43.
52. Chang, J.-L.; Tseng, G.-C.; Ni, C.-K.; Huang J.-D.; Chen, Y.-T. *J. Phys. Chem. A* **1999**, *103*, 6063.
53. Li, R.; Wu, J.-C.; Chang, J.-L.; Chen, Y.-T. *Chem. Phys.* **2001**, *274*, 275.
54. Mebel, A. M.; Chen, Y.-T.; Lin, S. H. *Chem. Phys. Lett.* **1996**, *258*, 53.
55. Mebel, A. M.; Chen, Y.-T.; Lin, S. H. *Chem. Phys. Lett.* **1996**, *105*, 9007.
56. Mebel, A. M.; Hayashi, M.; Lin, S. H. *Trends in Chemical Physics,* **1997**, *6*, 315.
57. Mebel, A. M.; Chen, Y.-T.; Lin, S. H. *Chem. Phys.* Lett. **1997**, *275*, 19.
58. Pibel, C. D.; Mcllroy, A.; Taatjes, C. A.; Alfred, S.; Patrick K.; Halpern, J. B. *J. Chem. Phys.* **1999**, *110*, 1841.
59. Liao, D.-W.; Mebel, A. M.; Chen Y.-T.; Lin, S. H. *J. Phys. Chem. A* **1997**, *101*, 9925.
60. Liao, D.-W.; Mebel, A. M.; Hayashi, M.; Shiu, Y. J.; Chen Y.-T.; Lin, S. H. *J. Chem. Phys.* **1999**, *111*, 205.
61. Tozer, D. J.; Handy, N. C. *J. Chem. Phys.* **1998** *109*, 10180.
62. Jamorski, C.; Casida M. E.; Salahub, D. R. *J. Chem. Phys.* **1996**, *104*, 5134.
63. Werner, H.-J.; Knowles, P. J. *J. Chem. Phys.* **1988**, *89*, 5803.
64. Knowles, P. J.; Werner, H.-J. *Chem. Phys. Lett.* **1988**, *145*, 514.
65. Werner, H.-J.; Knowles, P. J. *J. Chem. Phys.* **1985**, *82*, 5053.
66. Knowles, P. J.; Werner, H.-J. *Chem. Phys. Lett.* **1985**, *115*, 259.
67. *Gaussian 94* (Revision A.1), Frisch, M. J.; Trucks, G. W.; Schlegel, H. B.; Gill, P. M. W.; Johnson, B. G.; Robb, M. A.; Cheeseman, J. R.; Keith, T. A.; Petersson, G. A.; Montgomery, J. A.; Raghavachari, K.; Al-Laham, M. A.; Zakrzewski, V. G.; Ortiz, J. V.; Foresman, J. B.; Cioslowski, J.; Stefanov, B. B.; Narrayakkara, A.; Challacombe, M.; Peng, C. Y.; Ayala, P. Y.; Chen, W.; Wong, M. W.; Andres, J. L.; Replogle, E. S.; Gomperts, R.; Martin, R. L.; Fox, D. J.; Binkley, J. S.; Defrees, D. J.; Baker, J.; Stewart, J. P.; Head-Gorden, M.; Gonzalez, C.; Pople, J. A. Gaussian, Inc.: Pittsburgh PA, USA, 1995.
68. Farmanara, P.; Stert, V.; Radloff, W. *Chem. Phys. Lett*. **1998**, *288*, 518.
69. Berry, M. J. *J. Chem. Phys.* **1974**, *61*, 3114.
70. Moss, M. G.; Ensminger, M. D.; McDonald, J. D. *J. Chem. Phys*. **1981**, *74*, 6631.
71. Umemoto, M.; Seki, K.; Shinohara, H.; Nagashima, U.; Nishi,N.; Kinoshita, M.; Shimada, R. J. *Chem. Phys.* **1985**, *83*, 1657.
72. Donaldson, D. J.; Lenone, S. R. *Chem. Phys. Lett.* **1986**, *132*, 240.
73. Reilly, Y.; Xie, P. T. A.; Gordon, R. J. *Chem. Phys. Lett.* **1991**, *178*, 511.
74. Mo, Y.; Tonokura, K.; Matsumi, Y.; Kawasaki, M.; Sato, T.; Arikawa, T.; Reilly, P. T. A.; Xie, Y.; Yang, Y.-A.; Haung, Y.; Gordon, R. J. *J. Chem. Phys.* **1992**, *97*, 4815.
75. Huang, Y.; Yang, Y.-A.; He, G.; Gordon, R. J. J. *Chem. Phys.* **1993**, *99,* 2752.
76. Huang, Y.; Yang, Y.-A.; He, G.; Gordon, R. J. *J. Chem. Phys.* **1995**, *103,* 5476.
77. He, G.; Yang, Y.; Huang, Y.; Hashimoto, S.; Gordon, R. J. *J. Chem. Phys.* **1995**, *103*, 5488.
78. Tonokura, K.; Daniels, L. B.; Suzuki, T.; Yamashita, K. *J. Phys. Chem. A* **1997**, *101*, 7754.
79. Blank, D. A.; Sun, W.; Suits, A. G.; Lee, Y. T.; North, S. W.; Hall, G. E. *J. Chem. Phys.* **1998**, *108*, 5414.
80. Lin, S.-R.; Lin, S.-C.; Lee, Y.-C.; Chou, Y.-C.; Chen, I.-C.; Lee, Y.-P. *J. Chem. Phys*. **2001**, *114*, 160.
81. Nakayama, T.; Watanabe, K. *J. Chem. Phys.* **1964**, *40*, 558.
82. Ho, G. H.; Lin, M. S.; Wang, Y. L.; Chang, T. W. *J. Chem. Phys.* **1998,** *109*, 5868.
83. Mebel, A. M.; Jackson, W. M.; Chang, A. H. H.; Lin, S. H. *J. Am. Chem. Soc.* **1998**, *120*, 5751.
84. Currie, C. L.; Ramsay, D. A. *J. Chem. Phys*. **1966**, *45*, 488.
85. Callear, A. B.; Lee, H. K. *Trans. Faraday Soc*.**1968**, *64*, 308.
86. van der Bergh, H. E.; Callear, A. B. *Trans. Faraday Soc*. **1970**, *66*, 2681.
87. Nakashima, N.; Yoshihara, K. *Laser Chem*. **1987**, *7*, 177.
88. Tonokura, K.; Koshi, M. *J. Phys. Chem. A*, **2000**, *104*, 8456.
89. Hudgens, J. W.; Dulcey, C. S. *J. Phys. Chem*. **1985**, *89*, 1505.
90. Sappey, A. D.; Weisshaar, J. C. *J. Phys. Chem*.**1987**, *91*, 3731.
91. Kohn, D. W.; Chen, P. *Rev. Sci. Instrum*. **1992,** *63*, 4003.
92. Minsek, D. W.; Blush, J. A.; Chen, P. *J. Phys. Chem*. **1992**, *96*, 2025.

93. Blush, J. A.; Minsek, D. W.; Chen, P. *J. Phys. Chem*. **1992**, *96*, 10150.
94. Minsek, D. W.; Chen, P. *J. Phys. Chem*. **1993**, *97*, 13375.
95. Getty, J. D.; Burmeister, M. J.; Westre, S. G.; Kelly, P. B. *J. Am. Chem. Soc*. **1991**, *113*, 801.
96. Getty, J. D.; Kelly, P. B. *Chem. Phys*. **1992**, *168*, 357.
97. Getty, J. D.; Liu, X.; Kelly, P. B. *J. Phys. Chem.* **1992**, *96*, 10, 155.
98. Liu, X.; Getty, J. D.; Kelly, P. B. *J. Chem. Phys*. **1993**, *99*, 1522.
99. Getty, J. D.; Liu, X.; Kelly, P. B. *Chem. Phys. Lett*. **1993**, *201*, 236.
100. Wenthold, P. G.; Polak, M. L.; Lineberger, W. C. *J. Phys. Chem*. **1996**, *100*, 6920.
101. Locht, R.; Leyh, B.; Hottmann, K.; Baumg tel, H. *Chem. Phys*. **1997**, *220*, 207.
102. Locht, R.; Leyh, B.; Hottmann, K.; Baumg tel, H. *Chem. Phys*. **1997**, *220*, 217
103. Sheng, L.; Qi, F.; Tao, L.; Zhang, Y.; Yu, S.; Wang, C.-K.; Li, W.-K. *Int. J. Mass Spectrom. Ion Proc*. **1995**, *148*, 179.
104. Williams, B. A.; Cool, T. A. *J. Chem. Phys*. **1991**, *94*, 6358.
105. Herzberg, G. *Molecular Spectra and Molecular Structure. III*; Van Nostrand-Reinhold: New York, 1966.
106. Matsui, H.; Zhu, Y.-F.; Grant, E. R. *Laser Chem*. **1996**, *16*, 151.
107. Uy, D.; Davis, S.; Nesbitt, D. J. *J. Chem. Phys*. **1998**, *109*, 7793.
108. DeSain, J. D.; Thompson, R. I.; Sharma, S. D.; Curl, R. F. *J. Chem. Phys*. **1998**, *109*, 7803.
109. Houle, F. A.; Beauchamp, J. L. *J. Am. Chem. Soc*.**1978**, *100*, 3290.
110. Schultz, T.; Fischer, I. *J. Chem. Phys*.**1998**, *109*, 5812.
111. Kagramanov, N. D.; Ujszaszy, K.; Tamas, J.; Mal'tsev, A. K.; Nefedov, O. M. *Bull. Acad. Sci. USSR, Div. Chem. Sci*. **1983,** *7*, 1531.
112. Gilbert, T.; Fischer, I.; Chen, P. *J. Chem. Phys*. **2000**, *113*, 561.